Supporting Information

A novel Lanmodulin-Based Fluorescent Assay for the Rapid and Sensitive Detection of Rare Earth Elements

EXPERIMENTAL SECTION

SUPPLEMENTARY INTERPRETATIONS

SUPPLEMENTARY FIGURES

FigureS8. Fluorescence spectra of FITC-Hans-LanM (0.8 μg/ml in H_2O) upon addition of different concentrations of Dy^{3+}

FigureS9. Fluorescence spectra of FITC-Hans-LanM (0.8 μg/ml in H_2O) upon addition of different concentrations of Lu^{3+}

FigureS10. Fluorescence spectra of FITC-Hans-LanM (0.8 μg/ml in H_2O) upon addition of different concentrations of Y^{3+}

FigureS11. K^+ concentration effect on fluorescence intensity

FigureS12. Ca^{2+} concentration effect on fluorescence intensity

FigureS13. Na^+ concentration effect on fluorescence intensity

FigureS14. Mg^{2+} concentration effect on fluorescence intensity

FigureS15. Al^{3+} concentration effect on fluorescence intensity

FigureS16. Fe^{3+} concentration effect on fluorescence intensity

FigureS17. Mn^{2+} concentration effect on fluorescence intensity

EXPERIMENTAL SECTION

Expression of the fusion protein Hans-LanM

The constructed engineering bacteria were incubated with LB medium containing 30 mg/L kanamycin (10 g/L NaCl, 5 g/L yeast extract, 10 g/L tryptone) and cultured overnight at 220 rpm on a constant temperature shaker at 37°C. The bacterial culture was inoculated into fresh LB broth at a ratio of 1/100 and further incubated for 2 h until the

absorbance at 600 nM After that, the inducer IPTG was added to the culture at a final concentration of 1 mM and incubated overnight at 37°C to induce fusion protein expression. Then the culture medium was centrifuged at 4℃ for 20min at 5000rpm to obtain the bacterial cells. Add appropriate amount of lysis buffer (20mMtris solution) into the bacterial cells, freeze and thaw three times, then transfer to the crusher to crush twice, after crushing, centrifuge at 8000rpm for 15min, take the supernatant and dialyse it in deionised water, and change the water every 12h. After dialysis, the supernatant was centrifuged at 8000 rpm for 10 min, and the supernatant was lyophilised after centrifugation. The purified protein was analysed by SDS-polyacrylamide gel electrophoresis.

Gene sequence of SUMO:

ATGGGTCATCACCATCATCATCACGGGTCGGACTCAGAAGTCA
ATCAAGAAGCTAAGCCAGAGGTCAAGCCAGAAGTCAAGCCTG
AGACTCACATCAATTTAAAGGTGTCCGATGGATCTTCAGAGAT
CTTCTTCAAGATCAAAAAGACCACTCCTTTAAGAAGGCTGATG
GAAGCGTTCGCTAAAAGACAGGGTAAGGAAATGGACTCCTTA
AGATTCTTGTACGACGGTATTAGAATTCAAGCTGATCAGGCCC
CTGAAGATTTGGACATGGAGGATAACGATATTATTGAGGCTCA
CCGCGAACAGATTGGAGGT

Gene sequence of Hans-LanM:

ATGGCAAGTGGCGCGGATGCTTTGAAGGCGCTTAACAAAGAC
AATGACGATTCGCTGGAAATTGCAGAGGTAATCCACGCAGGC
GCAACTACGTTCACGGCAATCAACCCGGACGGAGACACAACTT
TGGAGAGCGGAGAGACGAAAGGACGCTTGACAGAAAAGGATT
GGGCTAGAGCTAATAAAGACGGGGACCAGACGTTGGAAATGG
ACGAATGGCTGAAGATCCTGAAAACTAGATTTAAAAGAGCCG
ATGCTAATAAGGATGGCAAATTAACGGCTGCGGAGTTGGATTC
CAAAGCGGGGCAAGGGGTATTGGTCATGATCATGAAAGGCAG
CGGCTGCTGA

Circular dichroism test conditions:

The light source was a 150 W xenon lamp, wavelength range 170 ~ 900 nm; wavelength accuracy ± 0.1 nm (170-400 nm), ± 0.5 nm (400 ~ 900 nm spectral repeatability, ± 0.05 nm (163 ~ 400 nm), ± 0.1 nm (> 400 nm); wavelength resolution: 0.1 nm: wavelengths of 170 ~ 900 nm interval were required to nitrogen purge, wavelength > 200 nm nitrogen flow rate of 5 L min-1. Nitrogen purge was required for the wavelength range of 170~900 nm, and the nitrogen flow rate was 2 L-min-1 for wavelength >200 nm and 5 L-min-1 for wavelength <200 nm.

SUPPLEMENTARY INTERPRETATIONS

The detailed explanation of the CD spectrum

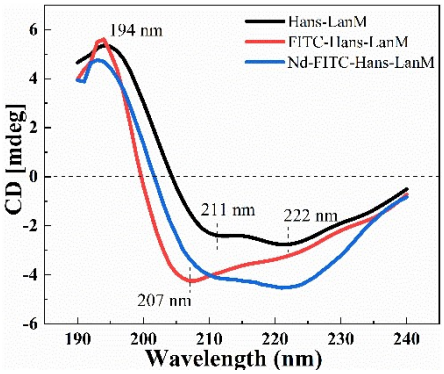

Supplementary Figure1. Circular dichroism determination of Hans-LanM, FITC-Hans-LanM and Nd-FITC-Hans-LanM

A "typical protein CD profile" refers to the characteristic circular dichroism (CD) spectrum observed for well-folded proteins, providing insights into their secondary structure content. Typical features include α-helices, β-sheets, and random coils. For proteins rich in α-helices, the CD spectrum typically shows a strong negative band around 222 nm and a weaker negative band around 208 nm, with their shape and intensity indicating the helical content. In contrast, proteins containing β-sheets usually display a negative band around 218 nm and a positive band around 195 nm, reflecting the presence of extended beta structures. Random coil structures have a less characteristic CD spectrum, often lacking distinct peaks and generally exhibiting weaker signals compared to structured proteins.

Hans-LanM exhibits a prominent positive peak around 194 nm, typically associated with random coil structures. The positive peak around 194 nm suggests a certain proportion of unordered structures. In the range of 205

nm to 240 nm, two connected negative peaks are observed, with maxima around 211 nm and 222 nm, primarily related to α-helical structures. The intensity of the negative peaks is directly proportional to the α-helix content.

The negative peak characteristics of FITC-Hans-LanM differ from those of Hans-LanM, with the maximum peak position appearing around 207 nm. This change may primarily relate to the addition of FITC, which, as a fluorescent label, interacts with the protein's amino acid residues, leading to conformational changes. This binding could alter the protein's folding state, affecting its secondary structure. Furthermore, the addition of FITC results in changes in the relative proportions of α-helices and β-sheets. FITC may cause local structural distortions, leading to shifts and intensity changes in the negative peaks observed in the CD spectrum. Additionally, the presence of FITC could introduce steric hindrance, interfering with normal protein folding, which may explain why the negative peak appears around 207 nm in FITC-Hans-LanM instead of the positions observed in Hans-LanM.

After adding Nd^{3+} to FITC-Hans-LanM, a significant decrease in the absolute intensity of the negative peak near 207 nm was observed, indicating a reduction in α-helix content. Following Nd^{3+} addition, Hans-LanM may have undergone conformational changes that reduced the stability of its α-helices, likely due to Nd^{3+} induced interactions interfering

with α-helical structure formation or maintenance, leading to decreased optical activity.

Simultaneously, the increase in the intensity of the negative peak near 222 nm may suggest that the reduction in α-helix content is accompanied by an increase in other secondary structures, such as dimeric structures. This change reflects the transition of the protein from a monomeric to a dimeric state under the influence of Nd^{3+}. Overall, the changes observed in the CD spectrum after the addition of Nd^{3+} illustrate the complexity of protein structure. The stability of the positive peak, the changes in negative peak intensity, and the formation of dimers indicate that Nd^{3+} promotes protein aggregation and refolding. This analysis helps to understand the crucial role of metal ions in regulating protein structure and function, providing a foundation for future research.

The determination of the detection limit

Supplementary Figure 2. The relationship between the concentration of Nd^{3+}

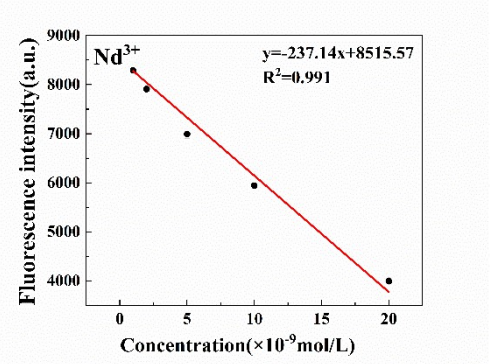

We established a relationship between the fluorescence intensity and concentration of known concentration samples by fitting a standard curve for Nd^{3+}, creating a correspondence between concentration and fluorescence signal. The linear fitting equation derived from the data is y=−237.14x+8515.57, with a correlation coefficient of R^2=0.991, This enables us to deduce the concentration of unknown samples by measuring their fluorescence intensity and using the standard curve. The R^2 value of the fitted standard curve for Nd^{3+} is approximately 0.991, indicating a strong linear relationship between the model and experimental data, which suggests a good fit. Therefore, when measuring the fluorescence intensity of unknown samples, we can confidently use this standard curve for concentration inference, and We can also calculate the detection limit based on the fitted standard curve. This process enhances the reliability and reproducibility of the results, demonstrating that our fitted model effectively describes the data and is suitable for prediction and analysis.

To calculate the limit of detection (LOD), multiple measurements of the fluorescence intensity of blank samples were conducted, and the standard deviation (SD) was computed. The fluorescence intensities of the blank samples were measured as 9095, 9052, and 9133. From these data, the average fluorescence intensity was determined to be 9093.33, with a standard deviation of approximately 40.6. Subsequently, the LOD was calculated using the following formula:

$$LOD = \frac{3 \times SD}{|slope|}$$

where the equation of the calibration curve of Nd^{3+} is given by y=−237.14x+8515.57, resulting in a slope of 237.14. Based on these calculations, the LOD was determined to be: LOD≈0.512 nM. This result indicates that the employed method is capable of effectively detecting low concentrations of samples, thereby providing a reliable foundation for subsequent analyses.

Supplementary Figure 3. The relationship between the concentration of La^{3+}

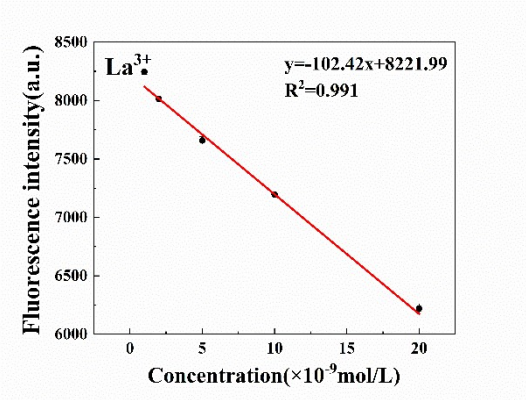

Supplementary Figure 4. The relationship between the concentration of Dy^{3+}

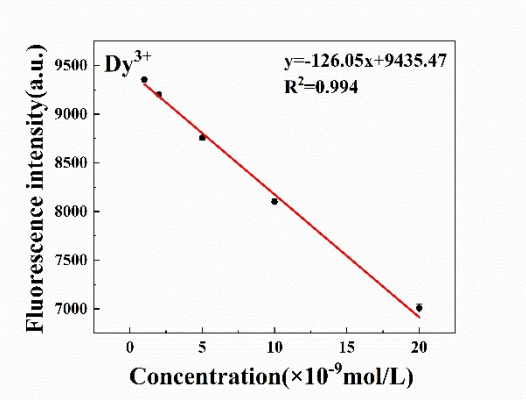

Supplementary Figure 5. The relationship between the concentration of Lu^{3+}

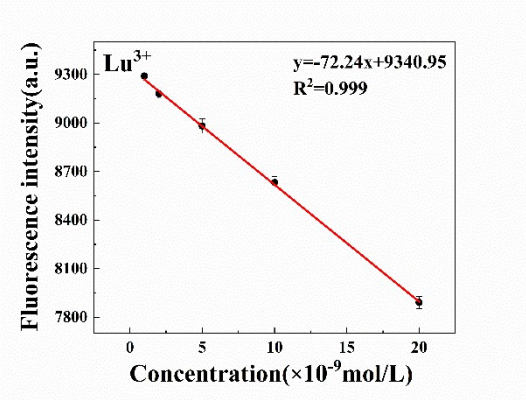

Supplementary Figure 6. The relationship between the concentration of Y^{3+}

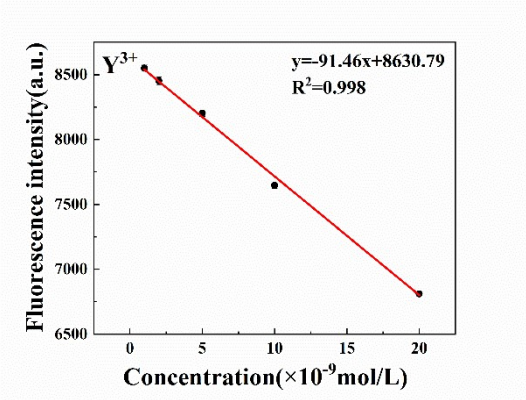

Supplementary Figure7. illustration of FITC binding with Hans-LanM

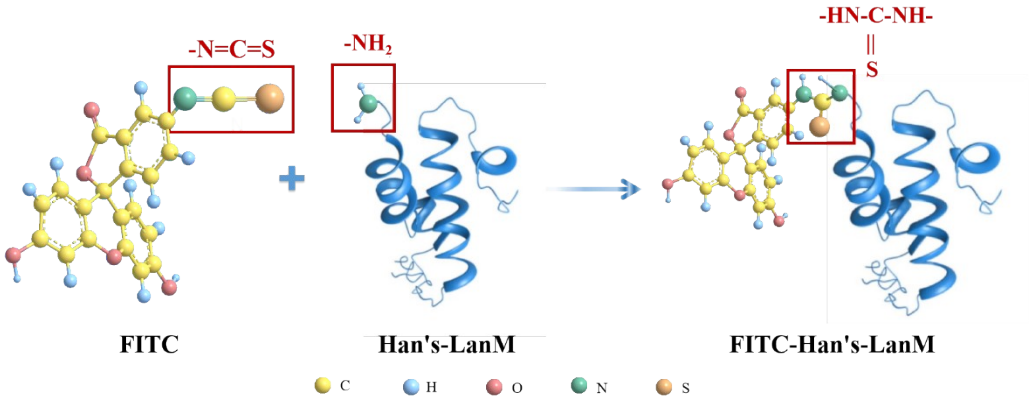

Supplementary Figure 8. Fluorescence spectra of FITC-Hans-LanM (0.8 μg/ml in H_2O) upon addition of different concentrations of Dy^{3+}

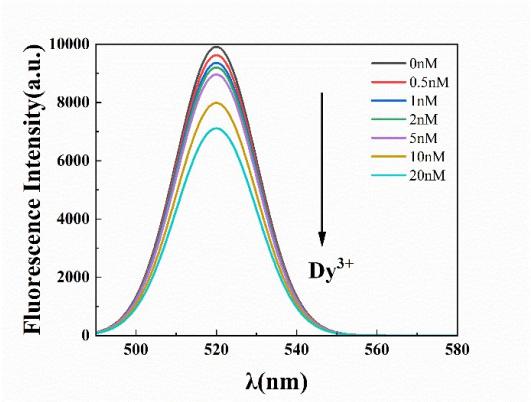

Supplementary Figure 9. Fluorescence spectra of FITC-Hans-LanM (0.8 μg/ml in H_2O) upon addition of different concentrations of Lu^{3+}

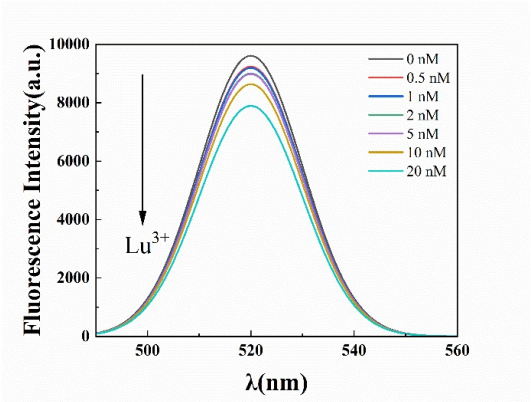

Supplementary Figure 10. Fluorescence spectra of FITC-Hans-LanM (0.8 μg/ml in H_2O) upon addition of different concentrations of Y^{3+}

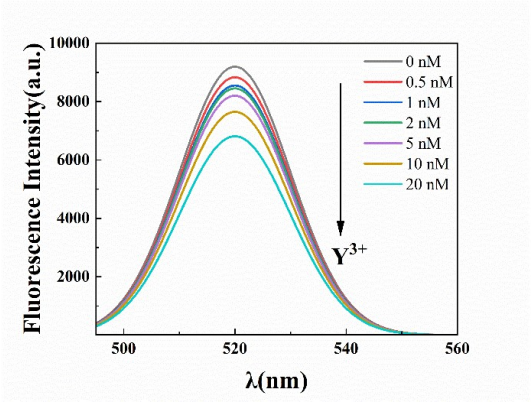

Supplementary Figure11. K^+ concentration effect on fluorescence intensity

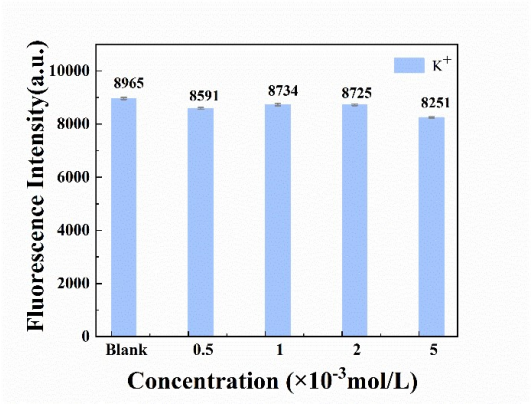

Supplementary Figure 12. Ca^{2+} concentration effect on fluorescence intensity

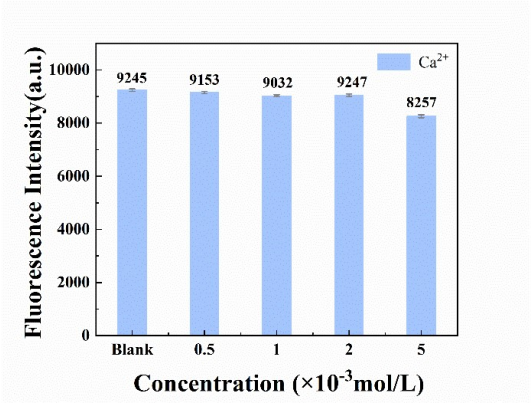

Supplementary Figure 13. Na^+ concentration effect on fluorescence intensity

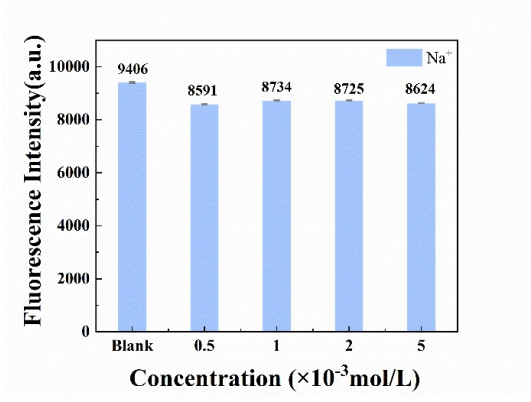

Supplementary Figure 14. Mg^{2+} concentration effect on fluorescence intensity

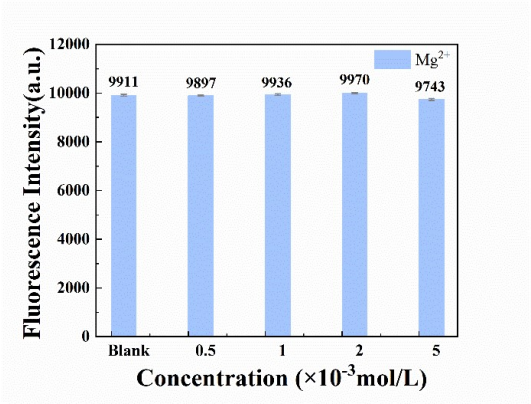

Supplementary Figure 15. Al^{3+} concentration effect on fluorescence intensity

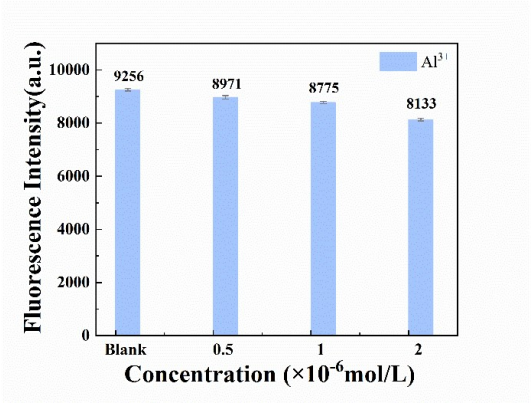

Supplementary Figure 16. Fe^{3+} concentration effect on fluorescence intensity

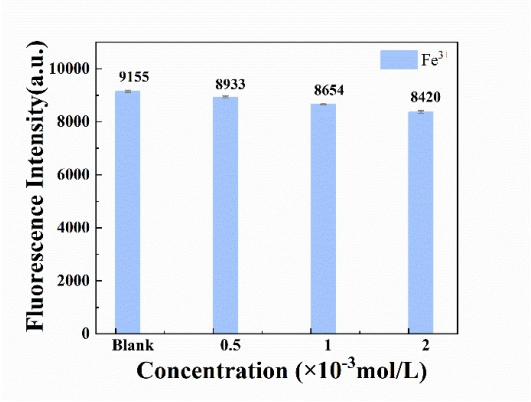

Supplementary Figure 17. Mn^{2+} concentration effect on fluorescence intensity